Effect of crystal-field splitting and interband hybridization on the metal-insulator transitions of strongly correlated systems

Alexander I. Poteryaev,[1] Michel Ferrero,[1] Antoine Georges,[1] and Olivier Parcollet[2]
[1]*Centre de Physique Théorique, UMR 7644, Ecole Polytechnique, CNRS, 91128 Palaiseau Cedex, France*
[2]*Institut de Physique Théorique, CEA, IPhT, CNRS, URA 2306, F-91191 Gif-sur-Yvette Cedex, France*
(Received 28 January 2008; revised manuscript received 22 April 2008; published 23 July 2008)

We investigate a quarter-filled two-band Hubbard model involving a crystal-field splitting, which lifts the orbital degeneracy as well as an interorbital hopping (interband hybridization). Both terms are relevant to the realistic description of correlated materials such as transition-metal oxides. The nature of the Mott metal-insulator transition is clarified and is found to depend on the magnitude of the crystal-field splitting. At large values of the splitting, a transition from a two-band to a one-band metal is first found as the on-site repulsion is increased and is followed by a Mott transition for the remaining band, which follows the single-band (Brinkman-Rice) scenario well documented previously within dynamical mean-field theory. At small values of the crystal-field splitting, a direct transition from a two-band metal to a Mott insulator with partial orbital polarization is found, which takes place simultaneously for both orbitals. This transition is characterized by a vanishing of the quasiparticle weight for the majority orbital but has a first-order character for the minority orbital. It is pointed out that finite-temperature effects may easily turn the metallic regime into a bad metal close to the orbital polarization transition in the metallic phase.

DOI: 10.1103/PhysRevB.78.045115 PACS number(s): 71.27.+a, 71.70.Ch, 71.30.+h, 71.10.Fd

I. INTRODUCTION

The Mott metal-insulator transition[1,2] plays a key role in the physics of strongly correlated electron materials. Over the last fifteen years, our theoretical understanding of this phenomenon improved considerably due to the development of the dynamical mean-field theory (DMFT) (Refs. 3 and 4). A number of model studies were performed in order to clarify the nature of the transition in both a single-orbital and multiorbital context.[5–13]

In the context of real materials, however, several important features must be considered, which are not always taken into account in model studies. This includes in particular two key aspects: (i) the breaking of orbital degeneracy by the crystalline environment and (ii) the existence of hopping terms coupling different orbitals on different sites of the crystal (interorbital hopping or hybridization). We note at this stage that the breaking of orbital degeneracy can correspond to a rather large energy scale (of order 1–2 eV) when one has in mind the crystal-field splitting between t_{2g} and e_g levels in a transition-metal oxide, but it can also correspond to a smaller energy scale (a small fraction of an electron volt) when considering, e.g., the trigonal splitting of the t_{2g} levels induced by a distortion of the cubic symmetry. In the former case, an effective model with fewer orbitals can often be considered, but in the latter case, all orbital components may still be relevant, albeit with different occupancies, and one has to use a model involving several orbitals with slightly different atomic level positions. In the present paper, we shall designate the lifting of orbital degeneracy by the generic term of "crystal-field splitting," but it is mostly the case where this is a small energy scale (e.g., trigonal splitting of the t_{2g} multiplet) that we have in mind for applications.

Indeed, the physical effects arising from the competition of crystal-field splitting and strong correlations have attracted a lot of attention recently, in particular in LDA+DMFT electronic structure studies of many different compounds. We now quote just a few examples. Pavarini *et al.*[14] pointed out that the lifting of cubic symmetry by the $GdFeO_3$-type distortion plays a key role in determining the metallic or insulating characters of d^1 transition-metal perovskites such as (Sr/Ca) VO_3 (small distortion, metals) and (La/Y) TiO_3 (larger distortion, insulators). Indeed, for a given value of the on-site Coulomb repulsion U, the lifting of the orbital degeneracy makes the insulating state more easily accessible.[9,10] Furthermore, correlation effects considerably enhance the effective crystal-field splitting, hence favoring orbital polarization (as also emphasized in Ref. 15 for these compounds). This correlation-induced enhancement of the effective crystal-field splitting and this increased orbital polarization have also been shown[16,17] to play a key role in the metal-insulator transition of V_2O_3, with the e_g^{π} component of the t_{2g} level much more occupied than the a_{1g} component in the insulating phase (see also the previous LDA+DMFT studies of V_2O_3 in Refs. 18 and 19).

Such effects were discussed, at a model level, in the pioneering paper of Manini *et al.*,[6] motivated by the physics of fullerene compounds. In this work, a model consisting of two orbitals occupied by one electron (quarter-filling) was considered and the combined effect of a crystal-field and of on-site repulsion was studied in the framework of DMFT. This work identified several phases, most notably a two-band metallic phase (with partial orbital polarization) and a one-band metallic phase (with full orbital polarization), as well as a fully orbitally polarized Mott insulating phase.

However, some questions of great importance were left unanswered by this early study. To quote just a few of these issues: (i) What is the nature of the metal-insulator transition in the different ranges of crystal field? (ii) How exactly does the crossover between a two-orbital Mott transition to a one-orbital Mott transition takes place? (iii) What is the effect of an interorbital hopping, always present in real materials, and

in particular does it wipe out the two-band metal to one-band metal transition within the metallic phase? and, finally, (iv), is it possible to obtain within DMFT the insulating phase with partial orbital polarization, which is expected from general strong-coupling arguments? (As we shall see, the answer is affirmative and this phase was overlooked in the DMFT study of Ref. 6).

All these questions are directly relevant to the understanding of real materials (e.g., V_2O_3 and Sr_2RuO_4) and to a better qualitative interpretation of the results of LDA+DMFT studies. The aim of the present article is to provide a detailed answer to these questions. This is made possible, in particular, by the recent development of numerical techniques for solving efficiently the DMFT equations, in particular continuous-time Monte Carlo algorithms.[20–23]

Let us point out that another related model study recently appeared, namely that of the two-orbital model at *half-filling* (i.e., two electrons in total).[8] In this case, the physical issues are quite different since one evolves from a two-orbital Mott insulator in the absence of crystal field to a band insulator at large crystal field (not a one-orbital Mott insulator as in our quarter-filled case). Also, this study did not consider the effect of an interorbital hopping. In this respect, our work and Ref. 8 can be considered quite complementary to one another.

Finally, we emphasize that the interplay between crystal-field splitting and strong correlations is made even more complex in the presence of Hund's coupling and exchange terms. In a study of $BaVS_3$ it was pointed out that when Hund's rule wins over crystal-field effects, one can observe a *compensation* between orbital populations rather than an enhanced orbital polarization.[24–26] The competition between Hund's coupling and crystal-field is also relevant to the physics of cobaltites,[27–30] ruthenates,[31–34] and monoxides under pressure.[35] In the present work, however, we focus on the interplay of crystal field and strong correlations and on the nature of the Mott transition, in the simplest possible context and consider only the effect of an on-site repulsion.

This paper is organized as follows: In Sec. II, we introduce the model and some notations. In Sec. III A we present the phase diagram and discuss qualitatively each phase. In Sec. III B, we discuss in details the insulating phases, using both an analytical strong-coupling method and complete numerical solution of the DMFT equations. In Sec. III C, we clarify the nature of the various phase transitions: from a two-band to a one-band metal and from a metal to a Mott insulator, in the different crystal-field regimes. Finally, in Sec. IV, we consider the effects of a finite interorbital hopping and also we discuss some finite-temperature effects in regimes where the two orbitals have very different quasiparticle coherence scales.

II. MODEL

We consider a minimal two-band Hubbard model with crystal-field splitting and interorbital hybridization, given by the Hamiltonian;

$$\hat{H} = \hat{H}_{\text{kin}} + \hat{H}_{\text{cf}} + \hat{H}_{\text{int}}, \tag{1}$$

with;

$$\hat{H}_{\text{kin}} = \sum_{\mathbf{k}} \sum_{\sigma m m'} \hat{\varepsilon}(\mathbf{k})_{mm'} d^{\dagger}_{\mathbf{k}\sigma m} d_{\mathbf{k}\sigma m'}, \tag{2a}$$

$$\hat{H}_{\text{cf}} = \frac{\Delta}{2} \sum_{i\sigma} (\hat{n}_{i\sigma 1} - \hat{n}_{i\sigma 2}), \tag{2b}$$

$$\hat{H}_{\text{int}} = \frac{U}{2} \sum_{i} \sum_{m\sigma \neq m'\sigma'} \hat{n}_{i\sigma m} \hat{n}_{i\sigma' m'}. \tag{2c}$$

In these expressions, i is a lattice-site index, $\mathbf{k}$ is the momentum in reciprocal space, $m=1,2$ is an orbital index, and $\sigma = \uparrow, \downarrow$ is a spin index. The sum in the interaction term runs over all orbital and spin indices except the case when $m = m'$ and $\sigma = \sigma'$ and therefore all intraorbital and interorbital Coulomb interactions are included. Δ is the crystal-field splitting between the two orbitals ($\Delta > 0$ favors the population of the second orbital,$m=2$), and U is the density-density Coulomb interaction between the two orbitals.

In this article, we focus on quarter-filling (i.e., one electron in two orbitals per lattice site), which is achieved by tuning appropriately the chemical potential μ. We consider only the density-density form of the interaction term, and we do not include the Hund's exchange, spin-flip, or pair-hopping terms. The motivation for neglecting these terms is to keep the Hamiltonian as simple as possible. Note however that, with one electron per site, the effect of these terms is expected to be small and acts basically as a renormalization of the on-site U (Refs. 11 and 12).

The kinetic term $\hat{H}_{\text{kin}}$ is a two-band tight-binding Hamiltonian on the three-dimensional cubic lattice (we will also use its Bethe lattice counterpart), which can be written (in $\mathbf{k}$ space) as

$$\hat{\varepsilon}(\mathbf{k}) = \begin{bmatrix} e(\mathbf{k}) & V(\mathbf{k}) \\ V(\mathbf{k}) & e(\mathbf{k}) \end{bmatrix}, \tag{3}$$

where diagonal elements correspond to the simple cubic lattice, and the off-diagonal ones have x^2-y^2 symmetry;

$$e(\mathbf{k}) = 2t(\cos k_x + \cos k_y + \cos k_z), \tag{4a}$$

$$V(\mathbf{k}) = 2\sqrt{3}V(\cos k_x - \cos k_y)\cos k_z. \tag{4b}$$

This corresponds to a hopping between identical orbitals on nearest-neighbor sites, equal to $-t$. The interorbital hopping connects orbitals $m=1$ and $m=2$ on next-nearest-neighbor sites and is equal in magnitude to $\sqrt{3}V/2$. It has a positive sign for the $[\pm 1, 0, \pm 1]$ neighbors and negative for the $[0, \pm 1, \pm 1]$ ones. This symmetry choice insures that, for all values of V, the on-site ($\mathbf{k}$ integrated) kinetic Hamiltonian is *diagonal in orbital space*. This is also the case of all local ($\mathbf{k}$ integrated) quantities in the interacting model, as can be checked by expanding the Green's function in power of V. Hence, our model is such that the choice of local-orbital basis set is adapted to the local crystal symmetry. Physically, the model [Eq. (3)] is a reasonable description, for example, of an e_g doublet split by the breaking of the cubic symmetry.

For zero hybridization, $V=0$, the density of states (DOS) is reduced to the DOS of the cubic lattice for both orbitals

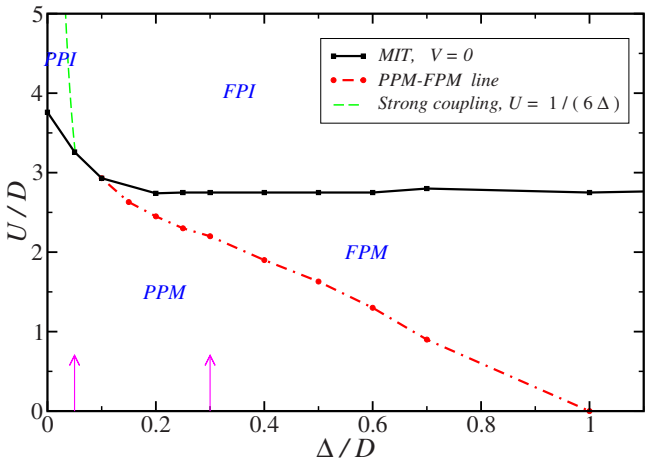

FIG. 1. (Color online) Zero-temperature phase diagram (paramagnetic phases) on the cubic lattice without hybridization ($V=0$), and for one electron per site. The solid (black) line separates metallic and insulating regions. The dot-dashed (red) line separates the partially polarized metal (PPM) and the fully polarized metal (FPM) (for details see text). The dashed (green) line is the result of the strong-coupling mean-field analysis [see Sec. III B 1 and Eq. (10)]: It separates the partially polarized insulator (PPI) from the fully polarized insulator (FPI). Arrows indicate the set of parameters used in Figs. 4 and 6. The ED solver was used.

shifted by $\pm\Delta/2$. We set the energy unit by $t=1/6$ or equivalently $D=1$, where D is the half-bandwidth.

We solve this model in the DMFT framework.[3] Since our main aim is to elucidate the nature of the metal-insulator transitions in this model, we focus in this article on the paramagnetic phases. The self-consistent impurity problem is solved with two numerical techniques: (i) Exact diagonalization (ED) as described in (Refs. 3 and 36), with a "star-geometry" for the bath hybridization function using five bath states per orbital degree of freedom; (ii) the recently introduced continuous time quantum Monte Carlo algorithm (CT-QMC) using an expansion in the impurity model hybridization function.[22,23] CT-QMC is more precise than ED and is necessary to establish the existence of the partially polarized insulator phase (see Sec. III B), as we shall discuss further below.

III. RESULTS IN THE ABSENCE OF INTERORBITAL HYBRIDIZATION

A. Zero-temperature phase diagram

The DMFT phase diagram of model [Eq. (1)] at quarter filling and without interorbital hybridization ($V=0$) is presented on Fig. 1. The effect of a nonzero V will be considered in Sec. IV. The general shape of this phase diagram can be easily anticipated by considering the various limiting cases:[6]

(i) For $\Delta=0$, one has a well documented two-band degenerate model. The model undergoes a correlation-driven Mott transition at a critical $U_c^{\Delta=0}\simeq 3.76$, which is close to the results obtained by other authors for the Bethe lattice (semicircular DOS with identical half-width $D=1$).[5–7]

(ii) For very large $\Delta \gg D$, the minority orbital (orbital $m=1$) is pushed to very high energy and becomes completely empty so that it can be ignored altogether. The quarter-filled two-band model thus reduces to a single-band model *at* half filling. This situation has been thoroughly studied within DMFT and yields a correlation-induced Mott transition at $U_c^{\Delta\to\infty}\simeq 2.75$. (see, e.g., Ref. 3 and references therein). The metal-insulator transition line (plain/black line on Fig. 1) interpolates between the limiting critical couplings corresponding to $\Delta=0$ and $\Delta=\infty$. The system is insulating above this line and is metallic below.

(iii) The noninteracting model ($U=0$) obviously has a transition between a two-band metal for $\Delta<D$ and a one-band metal for$\Delta>D$. For$\Delta=D$, the minority band crosses the Fermi level and becomes empty. This effective-band transition separating a two-band situation at low energy from a nondegenerate band can actually be followed through the phase diagram (dashed-dotted/red and dashed/green lines on Fig. 1), as we now discuss.

We note that we have not attempted to precisely determine whether the orbital polarization lines cross the metal-insulator transition (MIT) line at a single point or whether the orbital polarization line in the insulating phase and in the metallic phase hit the MIT boundary at slightly different locations.

In the absence of hybridization ($V=0$), we can use the orbital polarization as a faithful indicator of the transition between the two-band and a one-band regime. This quantity is defined as

$$\delta n = \frac{\langle \hat{n}_> \rangle - \langle \hat{n}_< \rangle}{\langle \hat{n}_> \rangle + \langle \hat{n}_< \rangle}, \tag{5}$$

in which $>$ and $<$ stand for the majority and minority orbitals, respectively, ($\langle \hat{n}_> \rangle > \langle \hat{n}_> \rangle$). At quarter filling and for $\Delta>0$, this reduces simply to $\delta n=\langle \hat{n}_2-\hat{n}_1 \rangle$.

As the crystal-field splitting is increased, one reaches a critical value at which the orbital polarization reaches $\delta n=1$, indicating a completely empty minority orbital. The line along which this happens in the (Δ, U) plane, is indicated by the dashed-dotted (red) line in the metallic phase and by the dashed (green) line in the insulating phase. Hence, four different phases are apparent on the phase diagram of Fig. 1: a partially polarized (two-band) metal (PPM), a fully polarized (one-band) metal (FPM), a partially polarized Mott insulator (PPI), and a fully polarized Mott insulator (FPI).

As already pointed out by Manini *et al.*,[6] and as clear from Fig. 1, the value of the crystal-field, at which the transition from the PPM to the FPM takes place, is strongly reduced by interactions. While it is set by the half-bandwidth at $U=0$, it is renormalized down by the quasiparticle weight $Z_>$ in the presence of interactions. Hence, a crystal-field splitting considerably smaller than the half-bandwidth can be sufficient to induce a two-band to one-band metal transitions.

It is important to realize, however, that the value of Δ needed to fully polarize the system vanishes only in the limit $U=\infty$. In other words, the orbitally degenerate Mott insulator at $\Delta=0$ has a *finite orbital polarizability*, even within the DMFT approach. Hence the PPI phase at large U and small

values of Δ exists. This point was incorrectly appreciated by Manini *et al.*,[6] largely for numerical reasons. Indeed, the ED algorithm is inappropriate to correctly capture the PPI phase. In the present article, we establish (Sec. III B) the existence of the partially polarized insulating phase within DMFT using both an analytical proof at strong-coupling limit and a complete numerical solution of the DMFT equations based on the new CT-QMC algorithm.

Let us point out that in this zero-temperature phase diagram, all the transitions are second order, except for the transition from the PPM to the PPI—which is second order for the majority orbital and first order for the minority orbital, as will be explained below in Sec. III C 2. At finite temperatures $T>0$, the MIT becomes first order throughout the phase diagram, as in canonical DMFT solutions, whereas the other transitions remain second order.

In the two following subsections, we describe in more details the nature of these different phases and we investigate the phase transitions between them.

B. Existence of the partially polarized insulator

1. Strong-coupling analysis: Kugel-Khomskii model

At strong coupling $U \gg D$ (or $U \gg t$), in the Mott insulating phases, an effective low-energy model can be derived, following Kugel and Khomskii[37] (see also Ref. 38). The low-energy Hilbert space contains only the four states $|i,m,\sigma\rangle$ with one electron on each site ($m=1,2$; $\sigma=\uparrow,\downarrow$). The effective Hamiltonian acting on these states reads,

$$\hat{H}_{\text{eff}} = -\Delta \sum_i \hat{T}_i^z + \sum_{\langle ij \rangle} \{J_s(\vec{S}_i\vec{S}_j) + J_o(\vec{T}_i\vec{T}_j) + J_m(\vec{S}_i\vec{S}_j)(\vec{T}_i\vec{T}_j)\}. \tag{6}$$

In this expression, $\langle ij \rangle$ denotes the bonds between nearest-neighbor sites and the spin and pseudospin (i.e., orbital isospin) operators are given by:

$$\vec{S}_i = \frac{1}{2}\sum_m d^\dagger_{i\sigma m}\vec{\tau}_{\sigma\sigma'}d_{i\sigma' m}, \tag{7a}$$

$$\vec{T}_i = \frac{1}{2}\sum_\sigma d^\dagger_{i\sigma m}\vec{\tau}_{mm'}d_{i\sigma m'}, \tag{7b}$$

in which $\vec{\tau}$ are the Pauli matrices. In particular, the z component of these operators (with eigenvalues $\pm 1/2$) is given by:

$$\hat{S}_i^z = \frac{1}{2}(\hat{n}_{i\uparrow 2} - \hat{n}_{i\downarrow 2} + \hat{n}_{i\uparrow 1} - \hat{n}_{i\downarrow 1}), \tag{8a}$$

$$\hat{T}_i^z = \frac{1}{2}(\hat{n}_{i\uparrow 2} + \hat{n}_{i\downarrow 2} - \hat{n}_{i\uparrow 1} - \hat{n}_{i\downarrow 1}). \tag{8b}$$

The (superexchange) couplings J_s, J_o, and J_m are given by[38]

$$J_s = J_o = \frac{J_m}{4} = \frac{2t^2}{U} \equiv J. \tag{9}$$

The particular symmetry between these couplings is due to the choice of a density-density interaction and to the neglect of the Hund's exchange.

At strong coupling, in the insulating phase, the DMFT solution of the original model [Eq. (1)] reduces to a static mean-field solution of Eq. (6). Focusing on the nonmagnetic phase ($\langle S_i^z \rangle = 0$), the orbital polarization $\delta n = 2\langle T^z \rangle$ is given by the self-consistent equation, at finite temperature $T=1/\beta$:

$$\delta n = \tanh\left[\frac{\beta}{2}(\Delta - \Delta_c \delta n)\right], \tag{10}$$

where

$$\Delta_c = \frac{zJ}{2} = z\frac{t^2}{U}, \tag{11}$$

is a critical value of the crystal-field splitting and z is the coordination number of the lattice (number of nearest neighbors). For the simple cubic lattice, with $z=6$ and half-bandwidth $D=zt$, this yields, $\Delta_c^{\text{CL}} = D^2/(6U)$, while for the large-connectivity Bethe lattice with nearest-neighbor hopping $t=D/(2\sqrt{z})$, one has: $\Delta_c^{\text{BL}} = D^2/(4U)$.

At zero temperature ($\beta=\infty$), the solution of Eq. (10) reads,

$$\delta n = \begin{cases} \Delta/\Delta_c, & \Delta < \Delta_c \\ 1, & \Delta \geq \Delta_c \end{cases}. \tag{12}$$

Hence, this shows that the orbitally degenerate insulator has a finite orbital susceptibility at $T=0$, $\chi_{\text{orb}} = 1/\Delta_c$, and that a finite crystal-field $\Delta = \Delta_c$ must be applied to fully polarize the insulating phase. The strong-coupling expression $\Delta = \Delta_c = D^2/(6U)$ for the cubic lattice corresponds to the dashed (green) line displayed on Fig. 1, separating the PPI from the FPI phases at $T=0$.

At finite temperature, a good approximation to the solution of Eq. (10) turns out to be;

$$\delta n \simeq \frac{\Delta}{\Delta_c}\frac{1}{1+\frac{2}{\Delta_c\beta}}. \tag{13}$$

Finally, we would like to emphasize that, when thinking of DMFT as an exact method in the limit of large lattice coordination $z\to\infty$, it is quite clear that a nonzero value of the critical Δ_c (and hence a finite extent of the PPI phase) is to be expected. Indeed, the orbital exchange coupling [Eq. (9)] scales as $1/z$ (since $t \propto 1/\sqrt{z}$), hence, the critical Δ_c is of the order of the exchange field between a site and all its neighbors, i.e., of order zJ, which remains $O(1)$ as $z\to\infty$. The *uniform* orbital susceptibility of the orbitally degenerate Mott insulator is indeed finite at $T=0$ (this should not be confused with the fact that the *local* susceptibility would scale as $1/z$ and hence vanish in the large-z limit).

2. Numerical solution: Importance of global moves in the quantum Monte Carlo algorithm

The analytical estimate at finite temperature [Eq. (13)] provides a very useful benchmark when solving numerically the DMFT equations for the original model in the strong-coupling regime. Indeed, it is actually nontrivial, from the numerical point of view, to successfully stabilize the partially polarized insulating phase. To achieve this, we have used the CT-QMC method, and it proved necessary to implement glo-

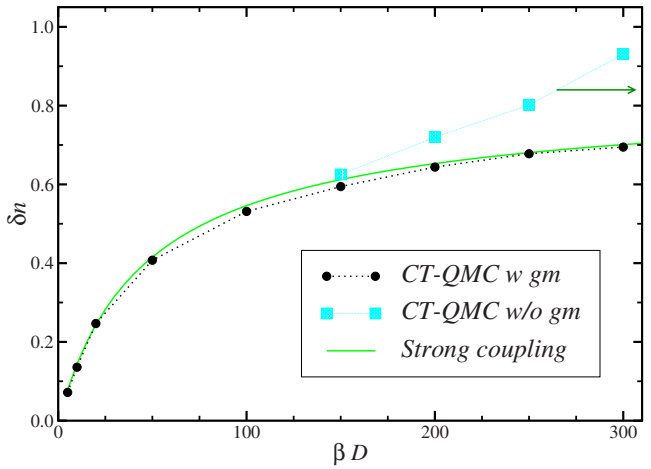

FIG. 2. (Color online) Temperature dependence of the orbital polarization, δn, for the cubic lattice in the PPI phase. Black dots are the CT-QMC data with the use of global moves (gm) in the spin and orbital space (see text for details). (Cyan) squares are the CT-QMC data without global moves. The solid (green) line is the strong-coupling result given by Eq. (10). The arrow shows the zero-temperature value of the polarization in the strong-coupling limit, $\delta n=0.84$. These results are obtained for $U=4$, $\Delta=0.035$, and using the CT-QMC solver.

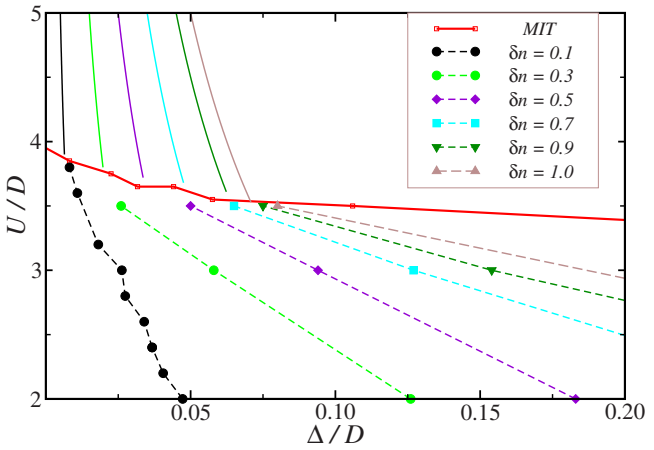

FIG. 3. (Color online) Metal-insulator transition (red) and isopolarization lines for the Bethe lattice. Different colors mark different values of the polarization (see legend). Dashed lines are ED results while solid lines are the solutions of Eq. (12) for constant polarization.

bal Monte Carlo moves, in addition to the Monte Carlo moves proposed in Ref. 8. In CT-QMC, a configuration is given by a collection of fermionic operators $c_{\alpha_1}(\tau_1)\ldots c_{\alpha_N}(\tau_N)$ at different imaginary times τ_i and the α_i are the fermionic species of the operators. The global moves are implemented by changing all α_i into a new set of α_i' and accepting the move with a probability satisfying the detailed balance condition. In this work, we have used two global moves that switch the spin $(\uparrow\leftrightarrow\downarrow)$ and the orbital $(1\leftrightarrow 2)$ indices. In the absence of these global moves, the calculation can be trapped in some regions of the phase space at low temperature, leading to a wrong (overestimated) value of the polarization.

This is illustrated in Fig. 2, which displays the temperature dependence of the polarization in the insulating phase, at small Δ. The result of Eq. (10) is compared to the CT-QMC results with and without global moves. One can see that without global moves, the polarization is bigger than its strong-coupling value, whereas the contrary is expected. This gives a clear indication that global moves are needed. When the correct implementation of the CT-QMC algorithm with global moves is used, the polarization falls below its strong-coupling value. Note that these results are actually obtained for an intermediate value of $U=4$, which shows that the range of validity of the strong-coupling approximation is actually quite extended. The agreement between the DMFT data with global moves and the strong-coupling result is seen to be excellent and both indubitably show the existence of the partially polarized insulator.

We have not been able (as in Ref. 6), when using the ED solver at $T=0$ in the insulating phase, to stabilize the partially polarized insulating solution at small Δ. This is probably because this solution is too delicate and involves a number of competing low-energy scales (J,Δ) to be faithfully reproduced given the simple parametrization and limited number of states in the effective bath, which can be handled within ED in a two-orbital context. However, ED performs quite well in the metallic phase and it is quite instructive to compare the isopolarization lines ($\delta n=$const) in the (Δ,U) plane, determined from ED, close to the metal-insulator transition to the strong-coupling result $\Delta/\Delta_c=\delta n$ (i.e., $U\Delta=zt^2\delta n$). This comparison is made in Fig. 3 in the case of the Bethe lattice (for simplicity). The ED data on the metallic side of the transition match very well to the strong-coupling form of the isopolarization lines on the insulating side. Thus, this provides a complementary way, starting from the metal, to document the existence of the PPI regime.

C. Metallic phases and the nature of the metal-insulator transition

We now turn to the metallic phases. There, the self-energies can be Taylor expanded at low-frequency as

$$\Re\Sigma_{\gtrless}(\omega+i0^+)=\Re\Sigma_{\gtrless}(0)+(1-1/Z_{\gtrless})\omega+\cdots, \quad (14)$$

in which $Z_>$ and $Z_<$ are the quasiparticle weights of the majority and minority bands, respectively. The quasiparticle weights, $Z_{\gtrless}=(1-\partial\Im\Sigma_{\gtrless}(i\omega)/\partial i\omega)^{-1}|_{\omega\to 0}$ were extracted from the imaginary frequency data with the use of third-order polynomials. The minority and majority Fermi surfaces in the metallic phase with PPM are determined, respectively, (for $V=0$) by:

$$e(\mathbf{k})=\mu+\frac{\Delta}{2}-\Re\Sigma_>(0)\equiv\mu_>, \quad (15a)$$

$$e(\mathbf{k})=\mu-\frac{\Delta}{2}-\Re\Sigma_<(0)\equiv\mu_<. \quad (15b)$$

The quantities $\mu_>,\mu_<$ can be viewed as effective crystal-field levels renormalized by interactions (or effective chemical potentials for each type of orbitals), and a renormalized crystal-field splitting can also be defined as

$$\Delta_{\text{eff}} \equiv \Delta + \Re\Sigma_<(0) - \Re\Sigma_>(0). \quad (16)$$

The various transitions are conveniently described in terms of $\mu_{\gtrless}$ and $Z_{\gtrless}$. On general grounds, there are two simple mechanisms by which a given orbital can undergo a transition from a metallic behavior to an insulating one:

(i) The quasiparticle weight Z may vanish at the MIT. This is the well-known Brinkman-Rice scenario, which is realized, e.g., within the half-filled single-band Mott transition within DMFT. It is also realized for degenerate orbitals with $\Delta=0$: $Z_>=Z_<$ vanishes continuously at $U_c^{\Delta=0}$.

(ii) It may also happen that either of the equations [Eq. (15a) and (15b)] fails to yield a solution, i.e., the "effective chemical potentials" $\mu_>$ or $\mu_<$ move out of the energy range $[-D,+D]$ spanned by $e(\mathbf{k})$. This, in turn, can happen in a continuous or in a discontinuous way.

1. Orbital polarization and metal-insulator transitions at large crystal field

We first consider values of the crystal-field splitting larger than$\gtrsim$0.1. Two successive transitions are observed as U is increased, from a two-band metal (PPM) to a single-band metal (FPM)—followed by a metal-insulator transition (FPM to FPI). Figure 4 (top panel) displays the quasiparticle residues $Z_>$,$Z_<$ and orbital polarization δn as U is increased at a fixed $\Delta=0.3$ (indicated by the arrow on Fig. 1). The lower panel of Fig. 4 displays $\mu_{\gtrless}$ and Δ_{eff}.

For $U<U_P$ ($\approx$2.2), in the two-band metallic phase (PPM), both quasiparticle weights decrease as U is increased, and the orbital polarization gradually increases.

At $U=U_P$, the polarization saturates to $\delta n=1$ and the minority band becomes empty. This happens following the mechanism (ii) above: the minority band effective level position $\mu_<$ hits the bottom of the band ($\mu_<=-D$ at $U=U_P$) and the renormalized crystal-field splitting reaches $\Delta_{\text{eff}}=+D$ [as clearly seen from Fig. 4 (lower panel)]. Simultaneously, $\mu_>$ vanishes at U_P and remains zero for $U>U_P$. This indicates that particle-hole symmetry is restored at low energy for the majority band throughout the FPM phase.

For $U_P<U<U_{\text{MIT}}$, the minority band is empty and becomes inactive. The remaining half-filled majority orbital forms a single-band metal and is subject to the local Coulomb interaction. This is illustrated in Fig. 5 where we plot the DOS of both orbitals. Note that the majority orbital very quickly becomes particle-hole symmetric over its full bandwidth as U increases. The quasiparticle weight of the majority band $Z_>$ is strongly reduced in this regime. Note that neither $Z_>$ nor $Z_<$ vanishes at the orbital polarization transition U_P. In fact, also the minority (empty) band self-energy remains linear in frequency at low energy in this regime, and a $Z_<$ can still be formally defined (as plotted on Fig. 4), although it no longer has the physical meaning of a quasiparticle spectral weight since there is no Fermi surface for that band. In particular, the increase of $Z_<$ in this region should not be interpreted as a decrease in the correlation effects.

Eventually, the transition from a single-band strongly correlated metal to a Mott insulator with full orbital polarization is found at $U=U_{\text{MIT}}$ ($\simeq U_c^{\Delta=\infty}\simeq 2.75$). The nature of this transition has been exhaustively described in the context of DMFT studies of the single-band model: $Z_>$ vanishes continuously at the critical point and the metal-insulator transition is second order (at $T=0$). The low-frequency majority

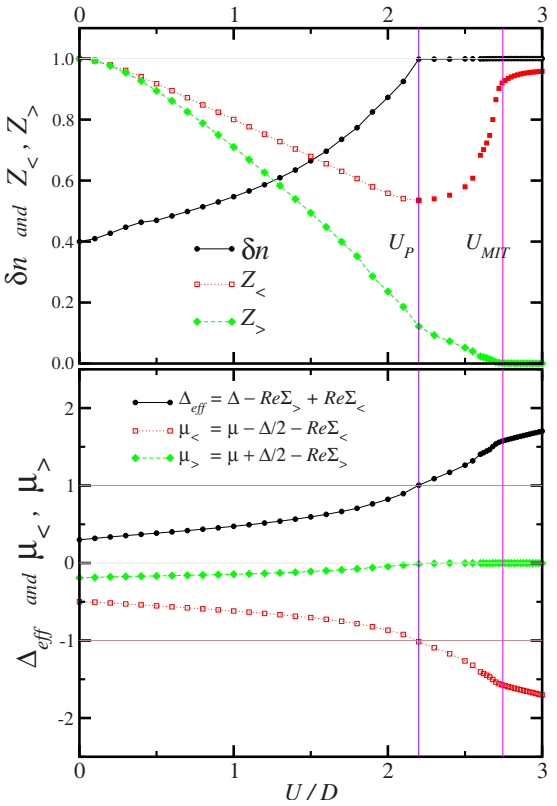

FIG. 4. (Color online) PPM-FPM-FPI transitions along the constant $\Delta=0.3$ line for the cubic lattice without hybridization ($V=0$). Top panel: Orbital polarization, δn, and QP residues, $Z_>$ and $Z_<$, are shown by (black) dots, filled (green) diamonds, and open (red) squares, respectively. Bottom panel: Effective crystal-field splitting, Δ_{eff}, and effective chemical potential for both bands, $\mu_>$ and $\mu_<$, are represented by (black) dots, filled (green) diamonds, and open (red) squares, respectively. The vertical lines show the full polarization (violet) and MIT transitions (magenta). The horizontal (brown) lines show the top and bottom of the bare band. The ED solver was used.

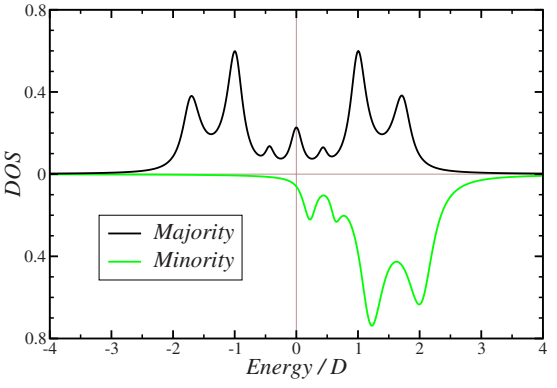

FIG. 5. (Color online) Density of states in the one-band metallic phase. The majority (minority) orbital is shown in the upper (lower) half of the plot. The ED solver was used with $U=2.4$ and $\Delta=0.3$.

self-energy $\Re\Sigma_>(\omega+i0^+)$ acquires a pole on the real frequency axis in the insulating phase. The location of this pole depends on the choice of the chemical potential within the insulating gap. For a specific choice (as done in Fig. 4), the pole is located at zero-frequency so that particle-hole symmetry is restored at low energy and the self-energy diverges as $\Re\Sigma_>(\omega+i0^+)\sim 1/\omega$.

It should be emphasized that the very small value of $Z_>$ in the one-band (FPM) metallic phase implies that the quasiparticles are actually quite fragile in that phase and can be easily destroyed by thermal effects. Hence, the orbital polarization transition at $U=U_P$ from a two-band to a one-band metal at $T=0$ may actually appear, at finite-temperature, as a transition between a two-band metal and a one-band incoherent "bad metal" (or quasi-insulator). We shall come back to this point in more detail in Sec. IV B.

2. Metal-insulator transition at small crystal field

In the small crystal-field regime ($\Delta \lesssim 0.1$), to the best of our numerical accuracy, there appears to be a simultaneous metal-insulator transition for both orbitals from a two-band metal (PPM) to a Mott insulator with partial orbital polarization (PPI). Note that in this region we needed to have recourse to finite-temperature Monte Carlo simulations.

The nature of the MIT has been well documented by previous DMFT studies in the degenerate case $\Delta=0$. At $T=0$, the transition is second order with a quasiparticle weight $Z_>=Z_<$ vanishing continuously at $U_c^{\Delta=0}$, while at $T>0$ this transition is first order.

On the top panel of Fig. 6, we display the quasiparticle weights $Z_>, Z_<$ as a function of U for $\beta=100$ and for a small value of $\Delta=0.05$, along with the orbital polarization δn. The MIT takes place at a critical coupling U_c^{Δ}, which is smaller than $U_c^{\Delta=0}$ (Fig. 1). Note that the data in Fig. 6 is obtained for a finite temperature and, therefore, the critical U_c^{Δ} is also smaller than its zero-temperature counterpart (shown in Fig. 1). The orbital polarization continuously increases with the interaction and does not approach the value $\delta n=1$ at the transition point. The minority orbital quasiparticle weight $Z_<$ remains larger than the majority one $Z_>$ in the metallic phase. Although it is a delicate issue numerically, our data appear to be consistent with a majority orbital quasiparticle weight $Z_>$, which vanishes continuously while $Z_<$ remains finite at the transition. Note that both the majority and minority orbital effective chemical potentials [Eqs. (15a) and (15b)] stay well within the energy band $[-D,+D]$ for all couplings in the metallic phase. The transition into the insulating phase for the minority orbital takes place by having $\mu_<$ jumping out of the energy band in an apparently discontinuous manner, as we now describe in more detail.

After the transition, the chemical potential μ can be placed (at $T=0$) anywhere within the charge gap, and therefore, the effective chemical potentials [Eq. (14)] are not longer defined in a unique manner. As documented in previous work[5,7] on the orbitally degenerate case within DMFT, we expect the majority orbital self-energy to have a pole on the real frequency axis, at a position that depends on μ. For a special choice of μ, this pole is located at $\omega=0$, which should correspond to a divergence of $\Sigma_>(\omega=0)$ and to a

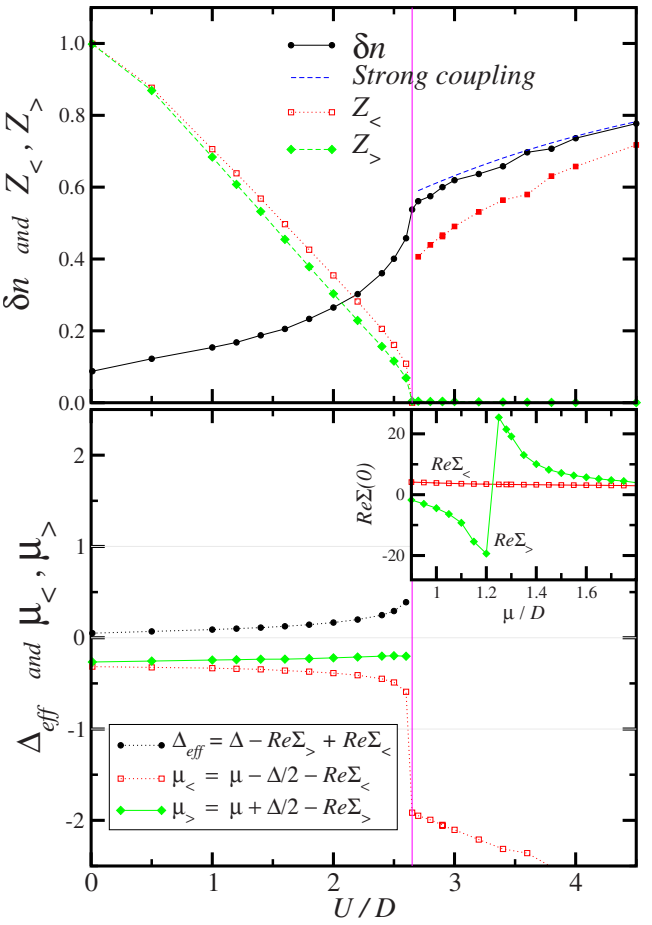

FIG. 6. (Color online) PPM-PPI transition along the constant $\Delta=0.05$ line for the cubic lattice without hybridization. Top panel: The (black) solid dots show the orbital polarization, δn. The QP residues, $Z_>$ and $Z_<$, are shown by the (green) filled diamonds, and (red) open squares, respectively. The (blue) dashed line is the strong-coupling result. Bottom panel: Effective crystal-field splitting, Δ_{eff}, and effective chemical potential for both bands, $\mu_>$ and $\mu_<$, are represented by (black) dots, filled (green) diamonds, and open (red) squares, respectively. The inset shows the real part of the self-energies at the first Matsubara frequency, $\Re\Sigma_{\gtrless}(i\pi/\beta)$, versus chemical potential within the gap for $U=3$. The vertical magenta line shows the MIT. The CT-QMC solver was used with $\beta=100$.

divergent self-energy $\sim 1/\omega$ at low frequency. In order to document this behavior, we plot in the inset of Fig. 6 the real part of the imaginary frequency self-energies, $\Re\Sigma_{\gtrless}(i\pi/\beta)$ at the first Matsubara point as a function of μ (for a given value of the interaction $U=3$). One can clearly see that the majority orbital self-energy, $\Re\Sigma_>(i\pi/\beta)$ becomes very big and changes sign at $\mu\sim 1.22$ while $\Re\Sigma_<(i\pi/\beta)$ stays constant within the gap. A careful scaling analysis shows that $\Sigma_>(\omega=0)$ indeed diverges at a critical value of μ. Together with the vanishing of $Z_>$, this shows that the transition for the majority orbital follows the standard DMFT scenario identical to the orbitally degenerate case. Furthermore, since $\Re\Sigma_<(i\pi/\beta)$ does not vary significantly when μ is varied within the gap, one can unambiguously define $\mu_<$ also in the insulating phase. In contrast, $\mu_>$ depends on the choice of μ. One should note here that the chemical potential, μ, defined

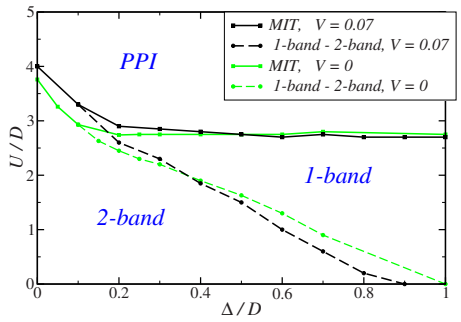

FIG. 7. (Color online) Zero-temperature phase diagram of the cubic lattice with hybridization $V=0.07$ and for one electron per site. The (black) solid line separates metallic and insulating regions. The (black) dot-dashed line separates the two-band and one-band metals. For the sake of comparison, the corresponding zero hybridization ($V=0$) lines are shown (in green). The ED solver was used.

in this way in the insulating phase continuously connects to the chemical potential in the metallic phase.

In Fig. 6 (bottom panel), we display these two quantities as a function of U, choosing for μ the special value at which $\Sigma_>$ behaves as $1/\omega$ at low frequency. From this plot, we see that the minority band becomes insulating because $\mu_<$ is jumping out of the energy band in a manner that appears as discontinuous (up to our numerical precision). Hence, in contrast to the orbital polarization transition of the large Δ case described above, the MIT at small Δ appears to occur in a discontinuous manner, as far as the minority band is concerned, while being continuous (Brinkman-Rice like) for the majority band. Note also that the minority orbital self-energy has a linear behavior at low frequency throughout the insulating phase.

Note that in this finite-temperature calculation, the orbital polarization never reaches $\delta n=1$ as U is further increased. From the strong-coupling calculation, we expect that it will saturate at $\delta n \simeq 0.987$ when $U \to \infty$. At zero temperature, however, there is a second-order transition at a finite critical value of U where the polarization reaches $\delta n=1$.

IV. EFFECT OF AN INTERORBITAL HYBRIDIZATION $V(\mathbf{k})$

A. Low-energy effective-band transition

In this section, we consider the effect of a finite hybridization (interorbital hopping $V(\mathbf{k}) \neq 0$). At low values of Δ, the metal-insulator transition is pushed to higher values of U when turning on a small V. While at larger values of Δ, the MIT line is less sensitive to V (as illustrated on Fig. 7). This is expected since at low Δ the interorbital hopping increases the kinetic energy in both bands while at higher Δ the hybridization with a band, which is already empty, has a smaller effect on the critical coupling. As we will discuss in more detail below, in the presence of the hybridization, the fully polarized phases (FPM and FPI) disappear. However, there is still a transition from a two-band to a one-band metal at low energy. This transition line is pushed up at low values of the crystal-field splitting because of the increase in kinetic energy. In noninteracting limit, the finite value of V acts as a

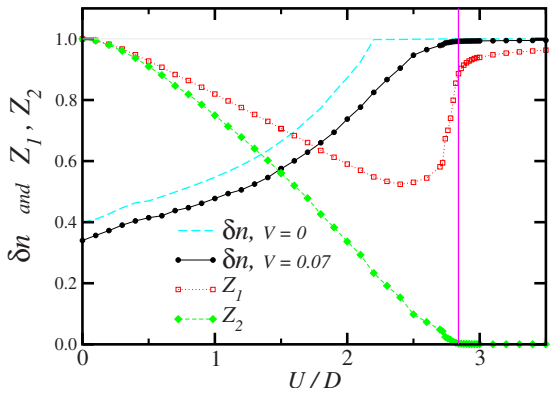

FIG. 8. (Color online) Orbital polarization δn (dots/black), quasiparticle weights Z_2 (green/filled diamonds), and Z_1 (red/open squares), as a function of U for a fixed value of $\Delta=0.3$ and a finite interorbital hybridization $V=0.07$. For the sake of comparison, the orbital polarization for $V=0$ is also displayed (cyan/dashed line). The vertical (magenta) line shows the MIT. The ED solver was used.

k-dependent enhancement of the crystal field Δ, and therefore, at small values of the interaction, the two-band to one-band transition line is below the corresponding $V=0$ line.

One should note that the majority (minority) band does not have a unique two (one) orbital character, and the band index $>$ ($<$) has to be distinguished from the orbital index two (one).

On Fig. 8, we display the quasiparticle weights and orbital polarization as a function of U, for a fixed value of V and a rather large crystal field $\Delta=0.3$. One clearly sees that the MIT follows a similar mechanism than in the $V=0$ case: only Z_2 vanishes continuously at the transition, while Z_1 is always finite.

A noticeable difference with the $V=0$ case is that the orbital polarization $\delta n=n_2-n_1$ does not reach saturation ($\delta n < 1$) before the MIT (Fig. 8). This is expected because the low-energy bands in the metallic state no longer have a unique (1,2) orbital character, as we now discuss.

In order to understand more precisely the nature of the metallic phase, we use the low-frequency expansion of the self-energies and we obtain the expressions of the low-energy majority and minority bands, which read,

$$2\omega_<(\mathbf{k}) = Z_1\varepsilon_{1\mathbf{k}} + Z_2\varepsilon_{2\mathbf{k}} + \sqrt{(Z_1\varepsilon_{1\mathbf{k}} - Z_2\varepsilon_{2\mathbf{k}})^2 + 4Z_1Z_2V_\mathbf{k}^2}, \tag{17a}$$

$$2\omega_>(\mathbf{k}) = Z_1\varepsilon_{1\mathbf{k}} + Z_2\varepsilon_{2\mathbf{k}} - \sqrt{(Z_1\varepsilon_{1\mathbf{k}} - Z_2\varepsilon_{2\mathbf{k}})^2 + 4Z_1Z_2V_\mathbf{k}^2}. \tag{17b}$$

In these expressions $\varepsilon_{1\mathbf{k}} \equiv e_\mathbf{k} - \mu + \Delta/2 + \Re\Sigma_1(0)$ and $\varepsilon_{2\mathbf{k}} \equiv e_\mathbf{k} - \mu - \Delta/2 + \Re\Sigma_2(0)$. The Fermi surface (set by $\omega=0$) is determined by the following condition (in which the weights $Z_{1,2}$ do not appear):

$$0 = \varepsilon_{1\mathbf{k}}\varepsilon_{2\mathbf{k}} - V_\mathbf{k}^2 \equiv [e_\mathbf{k} - \mu + \Delta/2 + \Re\Sigma_1(0)] \times [e_\mathbf{k} - \mu - \Delta/2 + \Re\Sigma_2(0)] - V_\mathbf{k}^2. \tag{18}$$

We recall that, when $V=0$, an orbital polarization transition

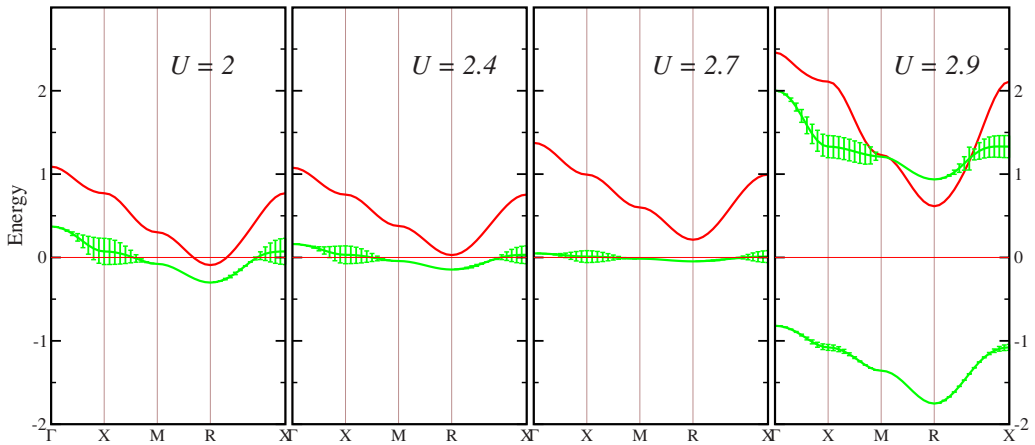

FIG. 9. (Color online) Linearized band structure along symmetry lines of the cubic lattice for different values of the interaction. We used $\Delta=0.3$, $V=0.07$, and the ED solver. Fatness shows a contribution of the spectral weight of the less occupied orbital ($m=1$) to the majority band (see text for details). $U=2.4$ corresponds to the value where the effective crystal-field splitting exceeds the bare bandwidth and the physical picture effectively becomes single band. The rightmost panel corresponds to the PPI solution and we used $\Re\Sigma_2(\omega+i0^+)=\Re\Sigma_2(0)+\Omega/\omega$ for the divergent orbital.

is first encountered at $U=U_P$, at which the Fermi-surface sheet corresponding to orbital 1 (determined by $\varepsilon_{1\mathbf{k}}=0$) disappears, since $\mu-\Delta/2-\Re\Sigma_1(0)$ reaches the band edge. In the presence of $V\neq 0$, a similar phenomenon occurs for the minority low-energy band $\omega_<(\mathbf{k})$: one of the two sheets, which constitute the solution of Eq. (18) ceases to exist. This is expected from continuity arguments in view of Eq. (18) and of the situation at $V=0$. This is furthermore demonstrated by Fig. 9, which displays the majority and minority low-energy bands $\omega_{\gtrless}(\mathbf{k})$ along the main directions in the Brillouin zone, as U is increased. It is clearly seen from this figure that for $U\simeq 2.4$ (before the MIT, which takes place at $U\simeq 2.8$), an effective band transition occurs between the two-band metal and a one-band metal at low energy. The critical coupling for this effective-band transition is slightly increased as compared to its value at $V=0$.

For $V=0$, the majority eigenstate $|\mathbf{k},>\rangle$ (corresponding to eigenvalue $\omega_>(\mathbf{k})$) has a unique orbital character $m=2$. In contrast, for $V\neq 0$, it has a component on both orbital 2 and orbital 1. As a result, the orbital polarization does not reach $\delta n=1$ (Fig. 8) at the effective band transition between a two-band and a one-band metal. On Fig. 9, we have used a "fat band" representation to illustrate this point: at each $\mathbf{k}$ point, we plot a bar whose extension is proportional to the matrix element $|\langle 1|\mathbf{k},>\rangle|^2$, measuring the projection of the less occupied orbital $m=1$ onto the majority band.

As U is increased beyond the effective band transition, one is left with a single effective low-energy band, characterized by a quasiparticle weight,

$$Z_>(\mathbf{k})=\frac{(\varepsilon_{1\mathbf{k}}+\varepsilon_{2\mathbf{k}})Z_1Z_2}{\varepsilon_{1\mathbf{k}}Z_1+\varepsilon_{2\mathbf{k}}Z_2}, \tag{19}$$

where $\mathbf{k}$ lies on the Fermi surface of the majority band [see Eq. (18)]. The subsequent Mott transition is characterized by a vanishing quasiparticle weight for the majority band $Z_>\sim Z_2\rightarrow 0$, as clearly seen from Fig. 8 and from the narrowing of that band in the third panel of Fig. 9.

The key conclusion of this section is that, even in the presence of a finite interorbital hopping, two distinct transitions are observed as U is increased (in the large crystal-field regime): first, a second-order transition from a metal with two active bands at low energy to a metal with only one active band at low energy, and followed by a Mott metal-insulator transition of the one-band type.

B. Orbital-selective coherence and the two-band metal to one-band bad-metal transition

We have seen above that, in a rather extended region of the metallic phase, the quasiparticle weight of the majority orbital is much smaller than that of the minority one. This is especially true close to the two-band to one-band metal transition, where $Z_2\ll Z_1$. This implies that thermal effects can easily destroy the fragile quasiparticles of the majority band. This has physical consequences, which may be important in practice. For example, the two-band metal to one-band metal transition at finite temperature may appear in practice as a quasi-metal-insulator transition or more precisely as a transition between a two-band metal and a bad (or incoherent) metal. This will happen when the temperature, at which the system is studied, is higher than the (small) quasiparticle coherence temperature of the majority band.

In order to illustrate this point, we performed finite-temperature studies for the following parameter values: $U=2$, $\Delta=0.3$, and $V=0.07$, which correspond to the two-band metallic regime, not very far from the two-band to one-band metal transition. For these parameters, the two quasiparticle residues are $Z_2=0.34$ and $Z_1=0.59$ (see Fig. 8). In Fig. 10, we display the imaginary part of the Green's functions (bottom) $\Im G_{1,2}(i\omega_n)$ and self-energies (top) $\Im\Sigma_{1,2}(i\omega_n)$ on the Matsubara axis, for different temperatures. In the insets of this figure, we display the extrapolated zero-frequency value $\Im\Sigma_{1,2}(i0^+)$, which is related to inverse quasiparticle lifetime and zero-frequency density of states, $\rho_{1,2}(0)\equiv-\Im G_{1,2}(i0^+)/\pi$, respectively.

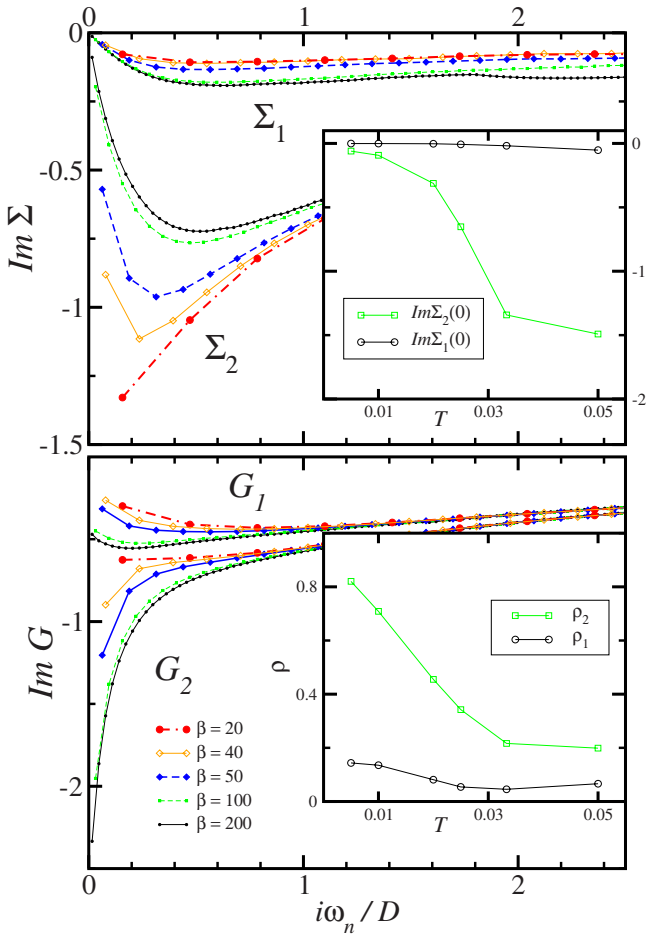

FIG. 10. (Color online) Top panel: Imaginary part of the self-energies, $\Re\Sigma_1(i\omega_n)$ and $\Im\Sigma_2(i\omega_n)$, for different temperatures (see legend for temperature coding). The inset shows the extrapolation to zero of the imaginary part of the self-energies, $\Im\Sigma_{1,2}(0)$, versus temperature. Bottom panel: Imaginary part of the Green's functions, $\Im G_1(i\omega_n)$ and $\Im G_2(i\omega_n)$, for different temperatures (the color coding is the same). The inset shows the density of states at the chemical potential $\rho_{1,2}(0)$ versus temperature. We used $U=2$, $\Delta=0.3$, $V=0.07$, and the CT-QMC solver.

It is seen from these figures that, while the minority orbital quantities have quite little temperature dependence, the majority orbital, in contrast, displays very strong temperature dependence. For example for $T\gtrsim 0.03$ (i.e., a rather low-energy scale as compared to the bandwidth), the majority orbital is clearly incoherent with a small quasiparticle lifetime and much reduced value of the local density of states. At those temperatures, the frequency dependence of the self-energy is clearly nonmetallic, extrapolating to a large value at zero frequency. Only at a low temperature $T\sim 0.01$ (200 times smaller than the bandwidth), the behavior of a coherent metal is recovered, with a linear Matsubara frequency dependence of $\Im\Sigma_2(i\omega_n)$ extrapolating to a small value at low frequency (corresponding to a large quasiparticle lifetime).

V. CONCLUSION

In this paper, we have investigated how a crystal-field splitting, by lifting orbital degeneracy, affects the Mott metal-insulator transition in the presence of strong on-site correlations. The study was performed on a simple two-orbital model at quarter filling (one electron per site), and we have also considered the effect of an interorbital hopping (hybridization), which is important for applications to real materials.

Within the metallic phase, a second-order transition from a two-band to a one-band metal takes place as the crystal field is increased. The critical value of the crystal-field splitting, at which this transition takes place, is considerably lowered for strong on-site repulsion (i.e., the effective crystal-field splitting is considerably enhanced). This transition has the nature of a effective band transition for the renormalized low-energy bands (i.e., the minority band is pushed up in energy and does not cross the Fermi energy anymore) and survives in the presence of an interorbital hopping.

The nature of the Mott metal-insulator transitions induced by on-site repulsion was found to depend on the magnitude of the crystal-field splitting. At high enough values of this splitting, the Mott transition is between a one-band metal and a one-band Mott insulator (conventional Brinkman-Rice scenario): only the majority orbital is involved, and the transition is second order and characterized by a vanishing quasiparticle weight for that orbital. At low values of the crystal-field splitting, the transition is from a two-band metal to a Mott insulator with *partial orbital polarization*. It takes place simultaneously for both orbitals: although the transition is still continuous for the majority orbital, it has a first-order character for the minority orbital. Elucidating these transitions and, in particular, establishing the existence of the partially orbitally polarized Mott insulator at low crystal fields was made possible by the recent development of the CT-QMC algorithm for the solution of the DMFT equations.

If a finite hybridization ($V\neq 0$) is taken into account, it is no longer possible to fully polarize the system. Therefore, the FPM and the FPI phases disappear. However, there is still a transition from a two-band to a one-band metal at low energy so that the introduction of a finite V does not modify the overall picture of the model.

We have also studied the influence of the temperature on the two-band metal just below the transition to the one-band metal. The temperature can easily drive the system into a regime where the quasiparticle weight of the majority band is destroyed and the system effectively becomes a single-band metal. Further increase of the temperature above the characteristic temperature of both bands leads the system into an incoherent (or bad) metal.

Our study has direct relevance for the interpretation of the metal-insulator transitions of transition-metal oxides (see Sec. I), often accompanied by an enhanced orbital polarization.

ACKNOWLEDGMENTS

We are very grateful to O.K. Andersen, S. Biermann, A. Rubtsov, and A. Lichtenstein for the discussions related to this work. We also thank V. Anisimov, F. Lechermann,

A. Millis, and P. Werner for the useful conversations. We acknowledge the support from CNRS, Ecole Polytechnique, the Agence Nationale de la Recherche (under contract *ETSF*), and the Marie Curie Grant No. MIF1-CT-2006-021820. This work was supported by a supercomputing grant at IDRIS Orsay under Project No. 071393 (for the ED results) and at CEA-CCRT under Project No. p588 (for the CT-QMC calculations).

[1] N. Mott, *Metal-Insulator Transitions* (Taylor and Francis, London, 1990).
[2] M. Imada, A. Fujimori, and Y. Tokura, Rev. Mod. Phys. **70**, 1039 (1998).
[3] A. Georges, G. Kotliar, W. Krauth, and M. J. Rozenberg, Rev. Mod. Phys. **68**, 13 (1996).
[4] G. Kotliar, S. Y. Savrasov, K. Haule, V. S. Oudovenko, O. Parcollet, and C. A. Marianetti, Rev. Mod. Phys. **78**, 865 (2006).
[5] T. Pruschke and R. Bulla, Eur. Phys. J. B **44**, 217 (2005).
[6] N. Manini, G. E. Santoro, A. Dal Corso, and E. Tosatti, Phys. Rev. B **66**, 115107 (2002).
[7] M. J. Rozenberg, Phys. Rev. B **55**, R4855 (1997).
[8] P. Werner and A. J. Millis, Phys. Rev. Lett. **99**, 126405 (2007).
[9] E. Koch, O. Gunnarsson, and R. M. Martin, Phys. Rev. B **60**, 15714 (1999).
[10] S. Florens, A. Georges, G. Kotliar, and O. Parcollet, Phys. Rev. B **66**, 205102 (2002).
[11] Y. Ōno, M. Potthoff, and R. Bulla, Phys. Rev. B **67**, 035119 (2003).
[12] J. E. Han, M. Jarrell, and D. L. Cox, Phys. Rev. B **58**, R4199 (1998).
[13] L. Laloux, A. Georges, and W. Krauth, Phys. Rev. B **50**, 3092 (1994).
[14] E. Pavarini, S. Biermann, A. Poteryaev, A. I. Lichtenstein, A. Georges, and O. K. Andersen, Phys. Rev. Lett. **92**, 176403 (2004).
[15] M. Mochizuki and M. Imada, Phys. Rev. Lett. **91**, 167203 (2003).
[16] M. S. Laad, L. Craco, and E. Müller-Hartmann, Phys. Rev. Lett. **91**, 156402 (2003).
[17] A. I. Poteryaev, J. M. Tomczak, S. Biermann, A. Georges, A. I. Lichtenstein, A. N. Rubtsov, T. Saha-Dasgupta, and O. K. Andersen, Phys. Rev. B **76**, 085127 (2007).
[18] G. Keller, K. Held, V. Eyert, D. Vollhardt, and V. I. Anisimov, Phys. Rev. B **70**, 205116 (2004).
[19] M. S. Laad, L. Craco, and E. Muller-Hartmann, Phys. Rev. B **73**, 045109 (2006).
[20] A. Rubtsov and A. Lichtenstein, JETP Lett. **80**, 61 (2004).
[21] A. N. Rubtsov, V. V. Savkin, and A. I. Lichtenstein, Phys. Rev. B **72**, 035122 (2005).
[22] P. Werner, A. Comanac, L. de' Medici, M. Troyer, and A. J. Millis, Phys. Rev. Lett. **97**, 076405 (2006).
[23] P. Werner and A. J. Millis, Phys. Rev. B **74**, 155107 (2006).
[24] F. Lechermann, S. Biermann, and A. Georges, Phys. Rev. Lett. **94**, 166402 (2005).
[25] F. Lechermann, S. Biermann, and A. Georges, Prog. Theor. Phys. Suppl. **160**, 233 (2005).
[26] F. Lechermann, S. Biermann, and A. Georges, Phys. Rev. B **76**, 085101 (2007).
[27] C. A. Marianetti, G. Kotliar, and G. Ceder, Phys. Rev. Lett. **92**, 196405 (2004).
[28] H. Ishida, M. D. Johannes, and A. Liebsch, Phys. Rev. Lett. **94**, 196401 (2005).
[29] C. A. Perroni, H. Ishida, and A. Liebsch, Phys. Rev. B **75**, 045125 (2007).
[30] C. A. Marianetti, K. Haule, and O. Parcollet, Phys. Rev. Lett. **99**, 246404 (2007).
[31] A. Liebsch and A. Lichtenstein, Phys. Rev. Lett. **84**, 1591 (2000).
[32] V. I. Anisimov, I. A. Nekrasov, D. E. Kondakov, T. M. Rice, and M. Sigrist, Eur. Phys. J. B **25**, 191 (2002).
[33] A. Liebsch and H. Ishida, Phys. Rev. Lett. **98**, 216403 (2007).
[34] X. Dai, G. Kotliar, and Z. Fang, arXiv:cond-mat/0611075 (unpublished).
[35] J. Kunes, A. V. Lukoyanov, V. I. Anisimov, R. T. Scalettar, and W. E. Pickett, Nat. Phys. **7**, 198 (2008).
[36] M. Caffarel and W. Krauth, Phys. Rev. Lett. **72**, 1545 (1994).
[37] K. Kugel and D. Khomskii, Sov. Phys. Usp. **25**, 231 (1982).
[38] D. P. Arovas and A. Auerbach, Phys. Rev. B **52**, 10114 (1995).